Article

Not peer-reviewed version

Fabrication of $ZnCo_2O_4$-$Zn(OH)_2$ Microspheres on Carbon Cloth for Photocatalytic Decomposition of Tetracycline

Sin-Ei Juang , Ning-Chien Chin , Yu-Cheng Chang * , Chia-Man Chou

Posted Date: 29 July 2024

doi: 10.20944/preprints202407.2266.v1

Keywords: $ZnCo_2O_4$-$Zn(OH)_2$ microspheres; carbon cloth; hydrothermal; thermal annealing; photocatalysts; methyl violet; tetracycline

Article

Fabrication of $ZnCo_2O_4$-$Zn(OH)_2$ Microspheres on Carbon Cloth for Photocatalytic Decomposition of Tetracycline

Sin-Ei Juang [1,2], Ning-Chien Chin [1,3], Yu-Cheng Chang [1,*] and Chia-Man Chou [4,5,6]

[1] Department of Materials Science and Engineering, Feng Chia University, Taichung 407102, Taiwan; juang5251@cgmh.org.tw (S.-E. J.) a111079@mail.tsmh.org.tw (N.-C. C.); yuchchang@fcu.edu.tw (Y.-C. C.);
[2] Department of Anesthesiology, Kaohsiung Chang Gung Memorial Hospital and Chang Gung University, College of Medicine, Kaohsiung, Taiwan;
[3] Department of Orthopedics, Antai Medical Care Corporation, Antai Tian-Sheng Memorial Hospital, Pingtung County, Taiwan;
[4] Department of Surgery, Taichung Veterans General Hospital, Taichung, 40705, Taiwan; cmchou@vghtc.gov.tw (C.-M. C.)
[5] College of Medicine, National Yang Ming Chiao Tung University, Taipei, 11221, Taiwan;
[6] Department of Post-Baccalaureate Medicine, National Chung Hsing University, Taichung, 40227, Taiwan
* Correspondence: yuchchang@fcu.edu.tw

Abstract: Zinc cobalt oxide-zinc hydroxide ($ZnCo_2O_4$-$Zn(OH)_2$) microspheres were successfully fabricated on carbon cloth via a sample hydrothermal method. The surface morphology of these microspheres and their efficacy in degrading methyl violet were further modulated by varying the thermal annealing temperatures. The manipulation of thermal annealing temperatures was pivotal in adjusting the porosity of $ZnCo_2O_4$-$Zn(OH)_2$ microspheres to amplify their photocatalytic performance. Various analytical techniques were utilized to evaluate the physical and chemical properties of the $ZnCo_2O_4$-$Zn(OH)_2$ microspheres, including field-emission scanning electron microscopy, energy-dispersive spectroscopy, X-ray diffraction, field-emission transmission electron microscopy, X-ray photoelectron spectroscopy, and UV-vis spectroscopy. Compared to untreated $ZnCo_2O_4$-$Zn(OH)_2$ microspheres, those subjected to thermal annealing exhibited increased specific surface area and light absorption capacity, rendering them highly effective photocatalysts under UVC light exposure. Subsequent studies have confirmed the superior performance of $ZnCo_2O_4$-$Zn(OH)_2$ microspheres as a reusable photocatalyst for degrading methyl violet and tetracycline. Additionally, trapping experiments during the photodegradation process involving $ZnCo_2O_4$-$Zn(OH)_2$ microspheres have identified hydroxyl radicals (·OH) and superoxide radicals ($\cdot O_2^-$) as the primary reactive species.

Keywords: $ZnCo_2O_4$-$Zn(OH)_2$ microspheres; carbon cloth; hydrothermal; thermal annealing; photocatalysts; methyl violet; tetracycline

1. Introduction

Spinel-structured photocatalysts are gaining attention for their cost-effectiveness, durability, and strong photoelectrochemical response, making them prime for enhancing solar energy capture [1–3]. Various AB_2O_4 spinels, such as $ZnFe_2O_4$ and $ZnCo_2O_4$, have been explored for applications ranging from gas sensing to energy storage and degradation of pollutants under visible light [4–6]. $ZnCo_2O_4$ is classified as a p-type semiconductor due to its spinel crystal structure and is notable for its versatility, including roles in Li-ion batteries, catalysis, and supercapacitors [7,8]. $ZnCo_2O_4$-based sensors have shown exceptional sensitivity to various gases, likely due to their high surface area [9]. The nanoparticles' morphology influences gas sensing performance, indicating a significant research interest in optimizing $ZnCo_2O_4$ sensors for higher sensitivity and lower operating temperatures [10,11]. Diverse synthesis methods like hydrothermal and microwave-assisted heating techniques have been developed, offering efficiency and cost-effectiveness for oxide material structures [12–15]. $ZnCo_2O_4$'s effective use in breaking down organic pollutants showcases its potential for

 doi:10.20944/preprints202407.2266.v1

environmental cleanup [16–18]. The evolution from bulk to porous structures, offering more active sites and better light absorption, marks a significant advancement [19]. The annealing-based self-sacrificial templating emerges as a cost-effective, high-performance method for fabricating these porous photocatalysts, emphasizing the importance of precursor selection in achieving superior product quality [16,20,21]. Previous studies have demonstrated the successful preparation of $ZnCo_2O_4$ nanostructures on carbon cloth for electrodes for supercapacitors and lithium-ion batteries [22–24]. However, their applications on carbon cloth for photocatalytic degradation remain infrequent.

Carbon cloth, a carbon filament textile, offers high conductivity, mechanical strength, and flexibility, making it ideal for flexible energy storage systems [25–27]. Despite a low surface area and few electroactive sites, carbon cloth is a flexible substrate for electrode materials [28–30]. Notably, Wang et al.'s oxidative method with hydrogen peroxide and sulfuric acid introduces oxygen-containing groups onto carbon cloth, enhancing its function [31]. Kordek et al., Liu et al., and Zhao et al. employed various complex activation methods to enhance the oxygen electrocatalytic activities of carbon cloth, each achieving improved performance through surface modification techniques, such as etching, calcining, plasma treatment, and doping with heteroatoms [32,33]. Therefore, surface modification technology can further improve carbon cloth's specific surface area and active sites, improving its application in various fields. Past research has shown that combining carbon cloth and $ZnCo_2O_4$ nanostructures creates a high-capacity, flexible anode with excellent cycle stability and rate performance, thus forming a highly flexible lithium-ion battery with excellent electrochemical properties [23,34]. In this study, the combination of carbon cloth and $ZnCo_2O_4$-$Zn(OH)_2$ microspheres is expected to be further used in the photocatalytic degradation of methyl violet and tetracycline, thereby simplifying the subsequent recycling process.

$ZnCo_2O_4$-$Zn(OH)_2$ microspheres fabricated on carbon cloth via a simplified hydrothermal process exhibited enhanced photocatalytic degradation of pollutants like methyl violet, thanks to optimized porosity from varied thermal annealing temperatures. Extensive characterization revealed that annealed microspheres offer superior surface area, light absorption, and charge carrier separation, making them highly effective under UVC light. These microspheres proved efficient and reusable photocatalysts, with superoxide and hydroxyl radicals identified as the major reactive species in pollutant degradation.

2. Results and Discussion

Figure 1 is a detailed schematic diagram illustrating the growing $ZnCo_2O_4$-$Zn(OH)_2$ microspheres on a carbon cloth substrate. Initially, carbon cloth undergoes a meticulous etching process using a mixture of sulfuric acid and hydrogen peroxide. This critical step creates a series of micropores on the surface, enhancing its texture and providing anchoring points that facilitate the subsequent nucleation and growth of $ZnCo_2O_4$-$Zn(OH)_2$ microspheres. After surface treatment, the carbon cloth was subjected to hydrothermal treatment, during which $ZnCo_2O_4$-$Zn(OH)_2$ microspheres began to form and adhere to the etched surface. The reaction process was performed at a controlled temperature of 120 °C and maintained for 2 h, ensuring uniform growth of microspheres. This carefully planned process resulted in the successful integration of $ZnCo_2O_4$-$Zn(OH)_2$ microspheres onto carbon cloth, laying the foundation for its potential application in photocatalytic degradation due to enhanced surface properties and synergistic effects between carbon cloth and $ZnCo_2O_4$-$Zn(OH)_2$ microspheres.

 doi:10.20944/preprints202407.2266.v1

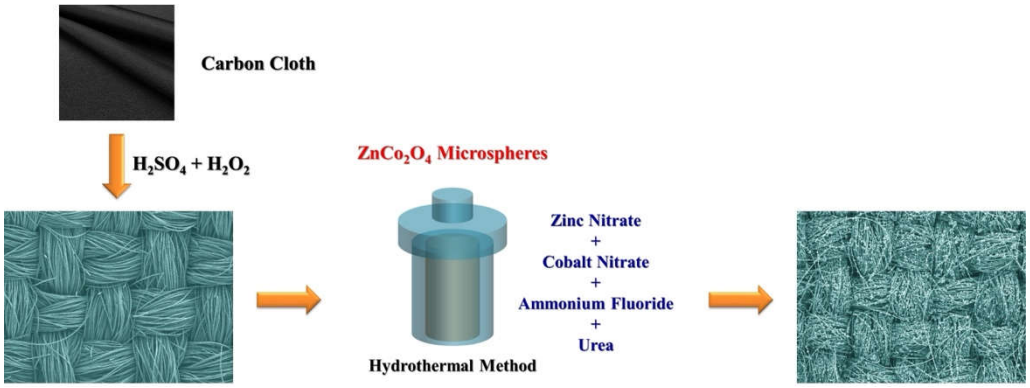

Figure 1. Diagram showing the $ZnCo_2O_4$-$Zn(OH)_2$ microspheres fabrication procedure on the carbon cloth.

Figure 2a and b show FESEM images of carbon cloth before and after soaking in a solution containing hydrogen peroxide and sulfuric acid. Before shaking, the carbon cloth surface is quite smooth. However, after soaking, the surface of the carbon cloth displays holes of various sizes. Subsequently, the two types of carbon are placed in a $ZnCo_2O_4$-$Zn(OH)_2$ reaction precursor at a reaction temperature of 120 °C for 2 h by a facile hydrothermal process, as shown in Figure 2 c and d. From these images, it can be observed that after soaking in the sulfuric acid and hydrogen peroxide mixed solution, the $ZnCo_2O_4$-$Zn(OH)_2$ microspheres that grow on the surface of the carbon cloth have a higher density. This result proves that soaking the carbon cloth in a solution containing hydrogen peroxide and sulfuric acid creates more pores on its surface and aids in the subsequent growth of $ZnCo_2O_4$-$Zn(OH)_2$ microspheres.

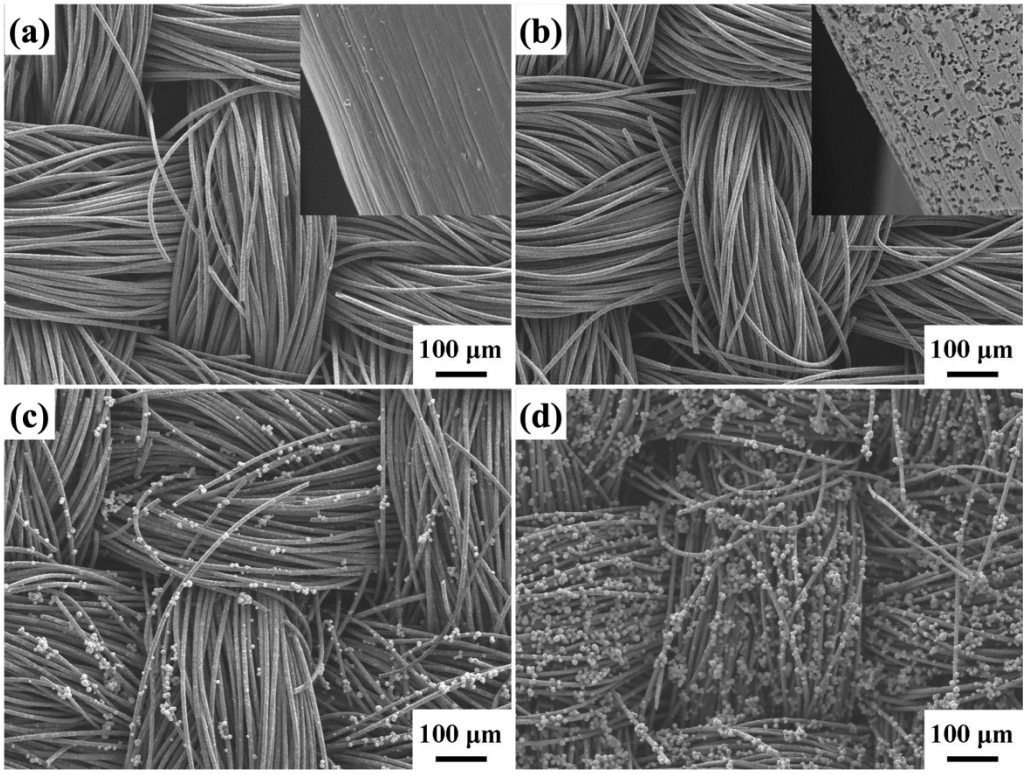

Figure 2. The FESEM images of (a) carbon cloth (without etching), (b) carbon cloth (etching), and $ZnCo_2O_4$-$Zn(OH)_2$ microspheres grown on the carbon cloth (c) without etching and (d) etching.

Additionally, high-resolution FESEM images (as seen in Figure 3a) depict the presence of $ZnCo_2O_4$-$Zn(OH)_2$ microspheres. The distribution of specific elements within these microspheres is further elucidated via FESEM-EDS elemental mapping, as showcased in Figure 3b-d. Examination of

 doi:10.20944/preprints202407.2266.v1

these images reveals that the microspheres are composed of zinc (Zn), cobalt (Co), and oxygen (O), with these components being uniformly distributed throughout. Consequently, this highlights the specific elemental composition of the $ZnCo_2O_4$-$Zn(OH)_2$ microspheres.

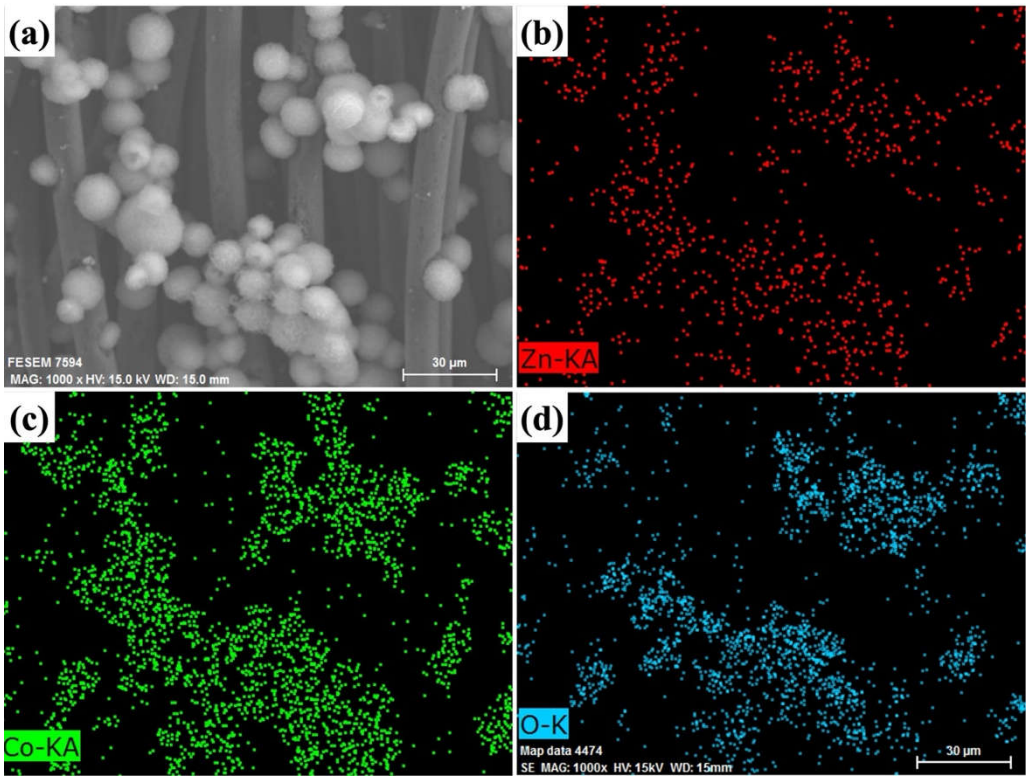

Figure 3. The (a) FESEM and (b-d) FESEM-EDS mapping images of $ZnCo_2O_4$-$Zn(OH)_2$ microspheres grown on the carbon cloth (etching).

Figure 4 shows scanning electron microscope images of $ZnCo_2O_4$-$Zn(OH)_2$ microspheres subjected to different thermal annealing temperatures for 2h. The thermal annealing temperatures are (a) without, (b) 450 ˚C, (c) 550 ˚C, and (d) 650 ˚C, respectively. As the annealing temperature rises, there is a progressive emergence of porosity on the surface. The surface morphology of the $ZnCo_2O_4$-$Zn(OH)_2$ microspheres remains unchanged compared to the unannealed samples, with the only noticeable difference being the appearance of porosity at an annealing temperature of 550˚C for 2 h. When the annealing temperature rises to 650˚C, it becomes apparent that some microspheres have collapsed. This occurrence drastically decreases the reactive surface area, negatively impacting the efficiency of subsequent photocatalytic reactions. The structural collapse observed at higher temperatures underscores the material's thermal instability, highlighting the necessity for meticulous optimization of the thermal annealing process to preserve the desired functional properties of the microspheres. Hence, the BET analyzer can assess the specific surface area of $ZnCo_2O_4$-$Zn(OH)_2$ microspheres before and after thermal annealing at 550 °C for 2 h. The surface area of the microspheres was measured at 20.78 m^2g^{-1} before thermal annealing, and following the annealing process, this value rose to 31.29 m^2g^{-1}. This result indicates that thermal annealing effectively enhances the specific surface area of the microspheres.

 doi:10.20944/preprints202407.2266.v1

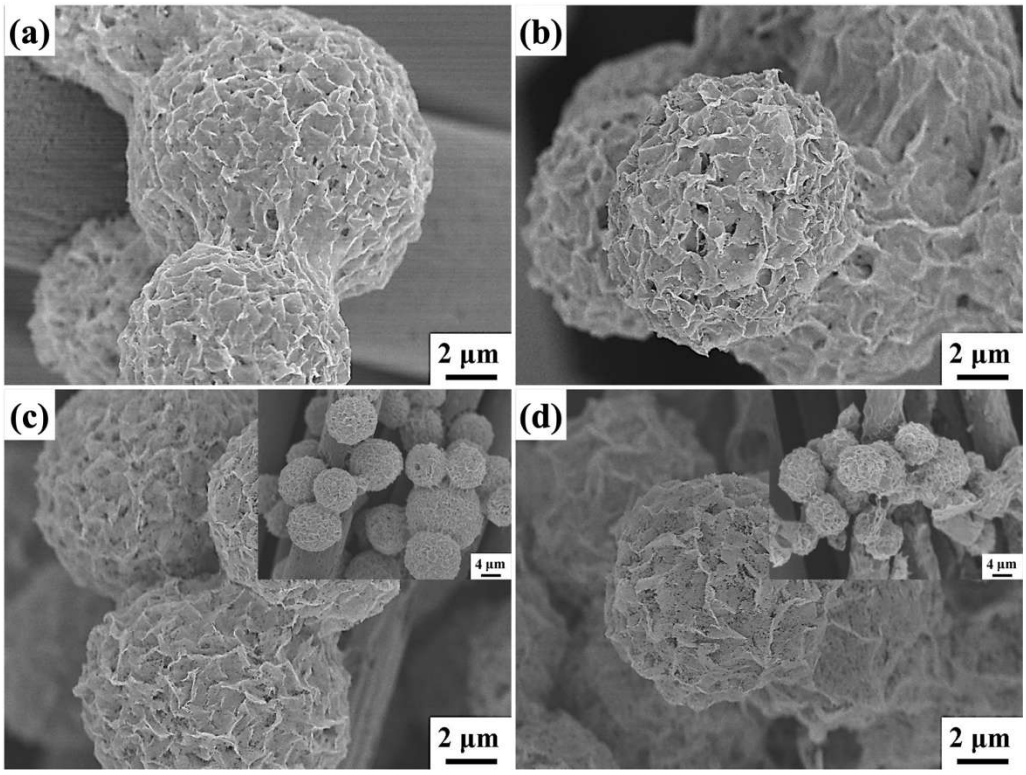

Figure 4. The FESEM images of $ZnCo_2O_4$-$Zn(OH)_2$ microspheres grown on the carbon cloth under the different annealing temperatures. The annealing temperatures are (a) without, (b) 450 ˚C, (c) 550 ˚C, and (d) 650 ˚C, respectively.

X-ray diffraction (XRD) was employed for the examination of the crystalline structure of the $ZnCo_2O_4$-$Zn(OH)_2$ microspheres (without thermal annealing) and $ZnCo_2O_4$-$Zn(OH)_2$ microspheres (thermal annealing at 550 °C for 2h), as shown in Figure 5. The diffraction angles of 29.6°, 35.5°, 43.3°, 47.5°, 57.2°, 58.0°, 60.9°, and 64.5° can be observed in $Zn(OH)_2$, corresponding to the (031), (211), (350), (181), (0120), (2111), (510), (152) and (1141) planes of orthorhombic $Zn(OH)_2$ (PDF No. 00-020-1437), respectively. The diffraction angles of 31.2°, 36.8°, 48.9°, and 65.2° can be observed in $ZnCo_2O_4$, corresponding to the (220), (311), (331), and (440) planes of cubic $ZnCo_2O_4$ (PDF No. 00-023-1390), respectively. It is evident that the peak intensity of $ZnCo_2O_4$ in $ZnCo_2O_4$-$Zn(OH)_2$ microspheres is weakened, indicating that the content of $ZnCo_2O_4$ is lower and the crystallinity is not as strong as that of $Zn(OH)_2$ when $Zn(OH)_2$ and $ZnCo_2O_4$ are combined. This result confirms the successful generation of $ZnCo_2O_4$-$Zn(OH)_2$ microspheres.

 doi:10.20944/preprints202407.2266.v1

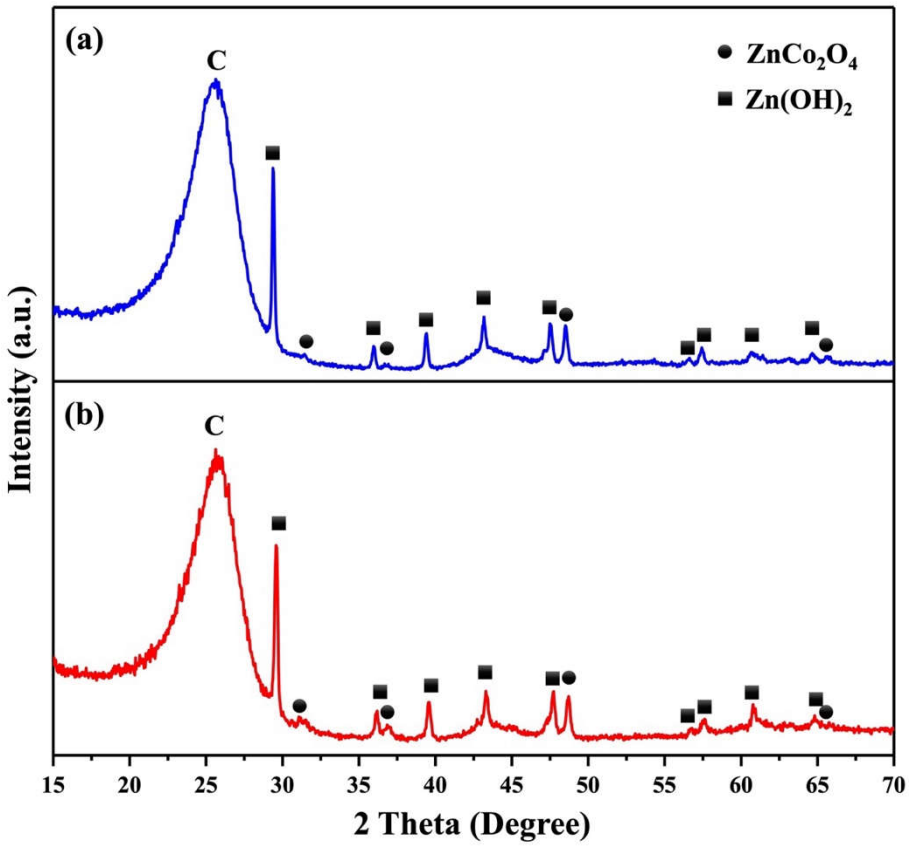

Figure 5. The XRD patterns of $ZnCo_2O_4$-$Zn(OH)_2$ microspheres grown on the carbon cloth (a) without thermal annealing and (b) thermal annealing at 550 °C for 2h, respectively.

The FETEM image in Figure 6a reveals a microspherical structure of $ZnCo_2O_4$-$Zn(OH)_2$, which aligns with the SEM results. This configuration is characterized by the arrangement of numerous sheets stacked on each other. The typical SAED pattern (Figure 6b) further confirms the polycrystalline nature of the $ZnCo_2O_4$-$Zn(OH)_2$ microsphere. The major diffraction ring closely matches the orthorhombic $Zn(OH)_2$ (PDF No. 00-020-1437) and cubic $ZnCo_2O_4$ (PDF No. 00-023-1390) crystal structures. The HRTEM image of the $ZnCo_2O_4$-$Zn(OH)_2$ microsphere (Figure 6c) displays crystal lattice fringes characterized by two discernible interplanar spacings: 0.302 nm and 0.244 nm. These can be attributed to the (031) crystallographic plane of the orthorhombic phase of $Zn(OH)_2$ and the (311) crystallographic plane of the cubic phase of $ZnCo_2O_4$. Figure 6d reveals the corresponding elemental mapping images of the $ZnCo_2O_4$-$Zn(OH)_2$ microsphere, showing the distribution of Zn, Co, and O elements. This result indicates that Zn, Co, and O define the $ZnCo_2O_4$-$Zn(OH)_2$ microsphere composition.

 doi:10.20944/preprints202407.2266.v1

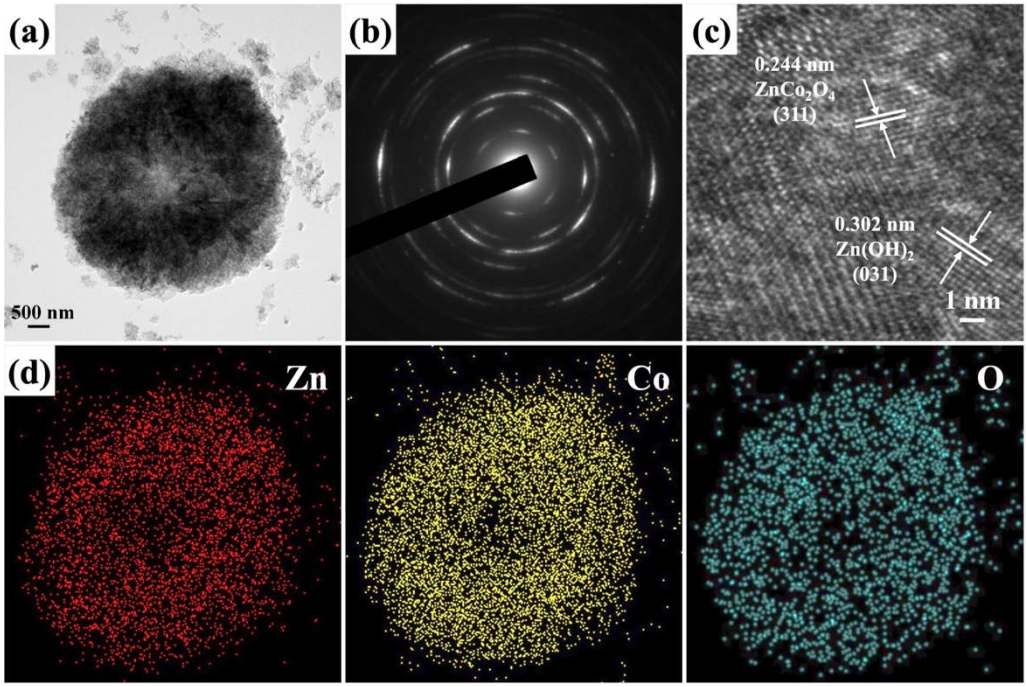

Figure 6. The (a) FETEM image, (b) SAED pattern, (c) HRTEM image, (d) EDS-mapping images of $ZnCo_2O_4$-$Zn(OH)_2$ microspheres grown on the carbon cloth under the annealing temperature of 550 °C.

To examine the elemental composition and valence distribution of the surface of $ZnCo_2O_4$-$Zn(OH)_2$ microspheres, an analysis utilizing X-ray photoelectron spectroscopy (XPS) was conducted. Figure 7a displays the full range XPS spectrum of $ZnCo_2O_4$-$Zn(OH)_2$ microspheres annealed at 550 °C, exhibiting distinct peaks corresponding to C, Zn, Co, and O. These peaks are consistent with the TEM-EDS observations, further confirming the presence of these elements. The carbon element is believed to have its source in the pump oil present in the vacuum system of the XPS equipment, carbon cloth, or an organic layer that has been applied to the surface of the sample. The high-resolution XPS spectrum (Figure 7b) of Zn 2p, showing peaks at 1020.9 eV and 1044.1 eV for Zn $2p_{3/2}$ and Zn $2p_{1/2}$, respectively, confirms the presence of Zn^{2+} in the $ZnCo_2O_4$-$Zn(OH)_2$ structure [35,36]. Figure 7c reveals the high-resolution XPS spectrum of Co 2p of $ZnCo_2O_4$, which can be deconvolved into four different states: Co^{3+} at 779.5 eV ($2p_{3/2}$) and 794.5 eV ($2p_{1/2}$), and Co^{2+} at 780.6 eV ($2p_{3/2}$) and 795.7 eV ($2p_{1/2}$). Additionally, two vibrational satellite peaks for Co^{2+} are located at 789.6 eV near the Co $2p_{3/2}$ band and 804.8 eV near the Co $2p_{1/2}$ band, consistent with previous literature [37,38]. The O 1s spectrum of the synthesized $ZnCo_2O_4$-$Zn(OH)_2$ microspheres (Figure 7d) reveals a primary peak at 529.5 eV corresponding to lattice oxygen (O_L), along with shoulder peaks at 530.8 eV and 532.1 eV attributed to surface hydroxyl groups (O_{OH}) and chemisorbed oxygen (O_C) [37,38].

 doi:10.20944/preprints202407.2266.v1

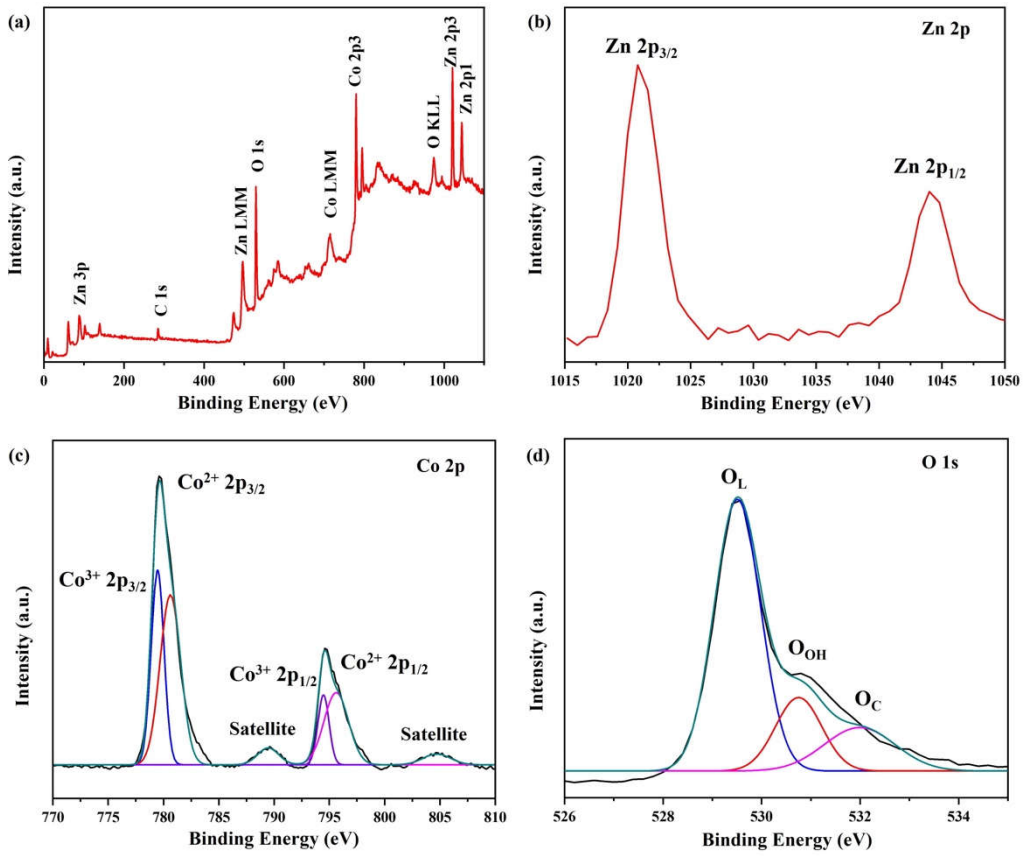

Figure 7. XPS (a) survey, (b) Zn 2p, (c) Co 2p, and (d) O 1s spectra of $ZnCo_2O_4$-$Zn(OH)_2$ microspheres under the annealing temperature of 550 °C.

To comprehend the correlation between the photocatalytic efficiency of $ZnCo_2O_4$-$Zn(OH)_2$ microspheres under different annealing temperatures, the photocatalytic activity in degrading methyl violet (MV), an organic pollutant commonly found in the textile industry was evaluated. $ZnCo_2O_4$-$Zn(OH)_2$ microspheres were grown on a 2.5 cm × 1.5 cm carbon cloth substrate as photocatalytic samples. The photocatalytic efficiency of $ZnCo_2O_4$-$Zn(OH)_2$ microspheres at different annealing temperatures was evaluated by the degradation of MV by UVC light (253 nm, 10 W), as shown in Figure 8a. The time variation of MV concentration was monitored by examining the change in maximum absorbance at 587 nm in UV-vis spectroscopy. The photodegradation percentages of MV were 58.0% (without annealing), 89.8% (450 ˚C), 91.7% (550 ˚C), and 78.6% (650 ˚C). When the annealing temperature was below 550 ˚C, a decrease in maximum absorbance was observed with increasing irradiation time and annealing temperature. $ZnCo_2O_4$-$Zn(OH)_2$ microspheres (550 ˚C) exhibited the highest photocatalytic activity in MV decomposition. The photocatalytic degradation process conformed to pseudo-first-order kinetics, and the plot of $-\ln(C/C_0)$ versus irradiation time (t) showed a pseudo-first-order linear relationship (Figure 8b), where C_0 is the initial concentration of MV and C is the actual concentration of MV at time t. The slope of the pseudo-first-order linear line is the apparent rate constant (k, min^{-1}) of the photocatalytic reaction. The rate constants of $ZnCo_2O_4$-$Zn(OH)_2$ microspheres at different annealing temperatures were calculated to be 0.03298 (without annealing), 0.05002 (450 ˚C), 0.08519 (550 ˚C), and 0.07241 (650 ˚C), respectively, in min^{-1}. $ZnCo_2O_4$-$Zn(OH)_2$ microspheres (550 ˚C) displayed the highest photocatalytic efficiency in MV photodegradation under UVC light irradiation. The rate constant (k) of $ZnCo_2O_4$-$Zn(OH)_2$ microspheres (550 ˚C) was about 2.58 times higher than that of the non-annealed ones. This phenomenon is attributed to the formation of porosity on the surface of $ZnCo_2O_4$-$Zn(OH)_2$ microspheres after annealing, which increases the active sites. However, when the annealing temperature is too high, it can cause the structure to collapse, leading to a decrease in active sites, which is consistent with the observations from SEM results.

 doi:10.20944/preprints202407.2266.v1

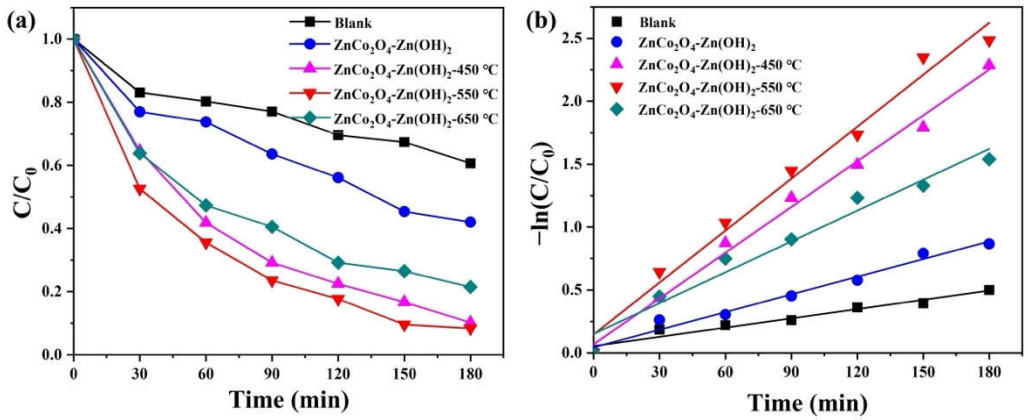

Figure 8. (a) Photocatalytic efficiency and (b) kinetic plot of as-prepared photocatalysts for MV solution under the UVC light irradiation.

We chose tetracycline (TC) as an antibiotic to illustrate that $ZnCo_2O_4$-$Zn(OH)_2$ microspheres can also be used for photocatalytic antibiotic degradation. Tetracycline (TC), a widely used antibiotic effective against various infections, is prevalent in water bodies due to its use as a growth promoter in aquaculture and insufficient removal by traditional wastewater treatments [39,40]. As demonstrated in Figure 9a, we observe the degradation rates of $ZnCo_2O_4$-$Zn(OH)_2$ microspheres before and after annealing when subjected to UVC light. The findings indicated that the microspheres that did not go through the annealing process had a degradation rate of 75.6%, whereas those that were annealed at a temperature of 550 °C exhibited a rate of 83.3%. Figure 9b represents the pseudo-first-order linear relationship of the $ZnCo_2O_4$-$Zn(OH)_2$ microspheres in the pre and annealing process. The reaction constants, corresponding to TC degradation over the non-annealed microspheres and those annealed at 550 °C, were determined to be 0.00794 and 0.00986 min^{-1}, respectively. Notably, the microspheres that underwent annealing at 550 °C showed superior photocatalytic activity, with their reaction constant being 1.24 times greater than their non-annealed counterparts when exposed to UVC light. This suggests an enhancement in photocatalytic efficiency due to the annealing process.

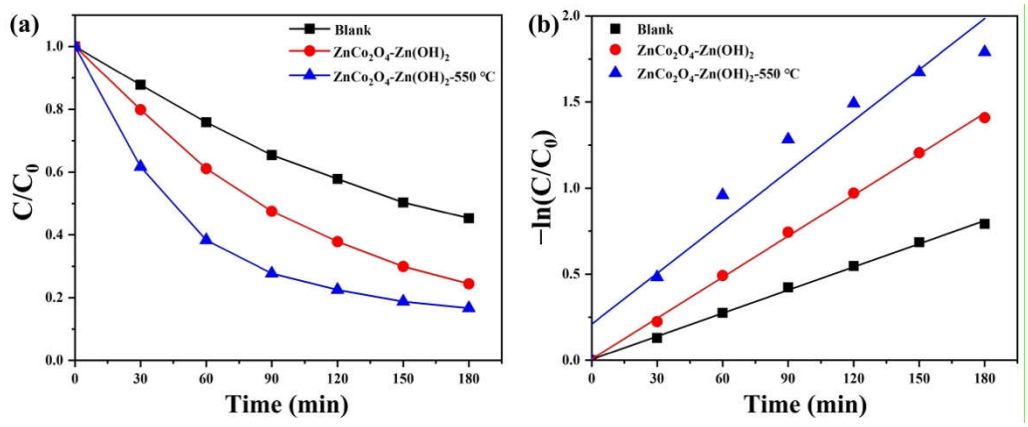

Figure 9. illustrates the (a) photocatalytic efficiency and (b) kinetic plot of the photocatalysts in treating TC solution under UVC light irradiation.

The recyclability of $ZnCo_2O_4$-$Zn(OH)_2$ microspheres (550 °C) was examined through repeated experiments involving the degradation of MV and TC solutions under UVC light irradiation, as shown in Figure 10. In the case of the MV solution (Figure 10a), the photocatalytic efficiency remained consistently high across four cycles, with efficiencies of 91.7%, 90.5%, 89.9%, and 87.4%, respectively. Similarly, the photocatalytic efficiency maintained a steady rate for the TC solution (Figure 10b), with efficiencies of 82.8%, 82.4%, 81.7%, and 80.9% across the four cycles. Even after four cycles of use, the decline in the photocatalytic efficiency of the $ZnCo_2O_4$-$Zn(OH)_2$microspheres was insignificant, demonstrating their durability and consistent performance. This result suggests that the $ZnCo_2O_4$-

 doi:10.20944/preprints202407.2266.v1

$Zn(OH)_2$ microspheres, heated at 550 °C, possess a long lifespan as photocatalysts, maintaining high activity and reusability. The $ZnCo_2O_4$-$Zn(OH)_2$ microspheres were also directly cultivated on a carbon cloth. In the meantime, the tested $ZnCo_2O_4$-$Zn(OH)_2$ microspheres (Figure 11) displayed remarkable consistency in the XRD patterns before and after degradation tests, validating their high resistance to photo-corrosion and stability. This result suggests that $ZnCo_2O_4$-$Zn(OH)_2$ microspheres have the promising potential for repeated use in practical applications, a highly desirable characteristic for sustainable and efficient photocatalysts. This resilience ensures their longevity and enhances their cost-effectiveness, making them a compelling choice for environmental applications. This unique growth method simplifies recycling and provides a stable and economical photocatalyst platform.

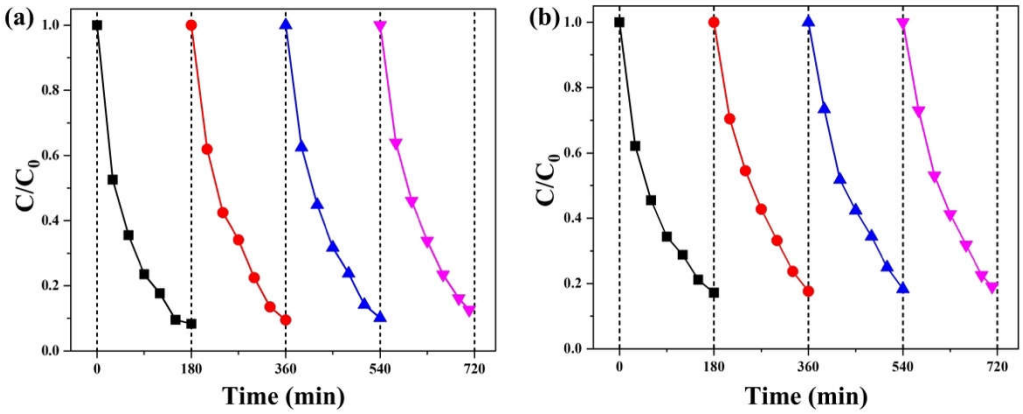

Figure 10. Recycle experiments of $ZnCo_2O_4$-$Zn(OH)_2$ microspheres for (a) MV and (b) TC solution under UVC light irradiation.

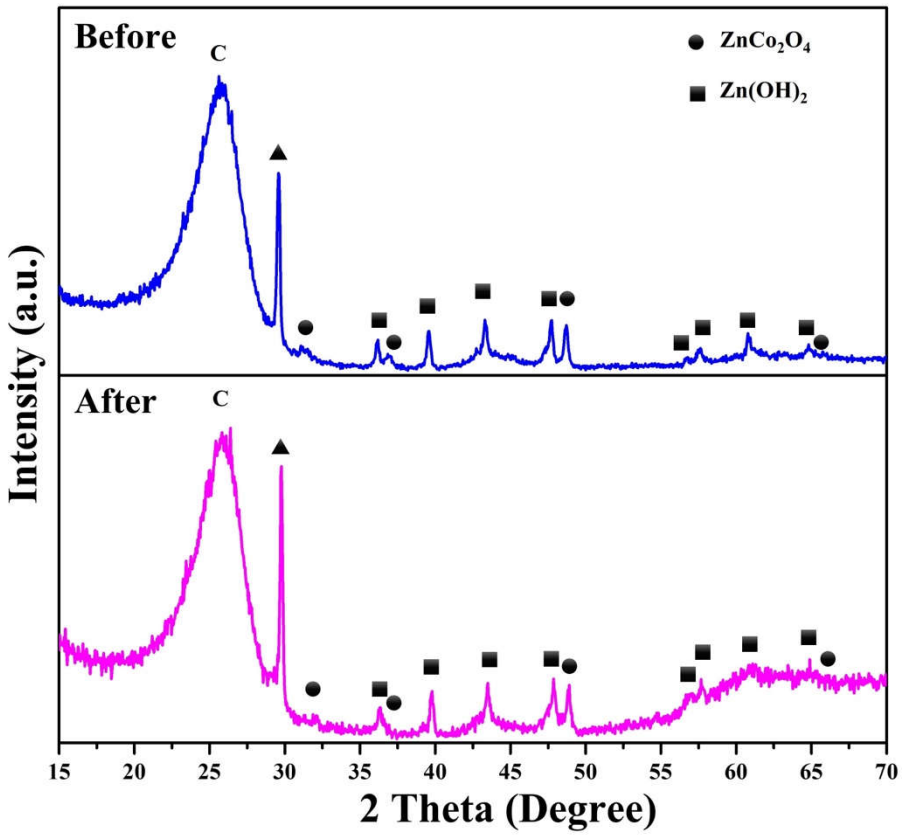

Figure 11. XRD patterns of $ZnCo_2O_4$-$Zn(OH)_2$ microspheres (550 °C) before and after four cycles of TC degradation.

 doi:10.20944/preprints202407.2266.v1

The optical properties of the $ZnCo_2O_4$-$Zn(OH)_2$ microspheres, both with and without thermal annealing, were examined using UV-visible spectroscopy. As shown in Figure 11a, the $ZnCo_2O_4$-$Zn(OH)_2$ microspheres that underwent thermal annealing at 550 °C demonstrated a significantly superior light absorption capacity within the spectral range spanning from 250 to 800 nm compared to those that did not undergo annealing. The improved light absorption spectrum observed in the annealed microspheres offers advantages for maximizing solar energy utilization, thereby enhancing the photocatalytic degradation process. The energy band gaps (E_g) were established utilizing the Tauc relationship, represented by the equation: $\alpha h\nu = A(E_g - h\nu)^{1/n}$ [41,42]. In the provided equation, A, α, ν, E_g, and h represent constants: the constant, the absorption coefficient, the frequency of light, the band gap energy, and Planck's constant, respectively. The variable "n" denotes a property of the semiconductor material, taking a value of 2 for indirect bandgap semiconductors and 1/2 for direct bandgap semiconductors, as illustrated in Figure 11b. The energy band gap value of the $ZnCo_2O_4$-$Zn(OH)_2$ microspheres, both pre and post-annealing, was computed to be approximately 2.42 eV. This data validates that the energy gap remains relatively constant throughout the thermal annealing process. Moreover, a straightforward thermal annealing technique can offer a high specific surface area and a more extensive optical absorption spectrum at a suitable temperature. This method significantly enhances the photocatalytic degradation of MV or TC solutions, improving their overall performance and effectiveness.

Four radical scavengers were introduced into the photocatalytic reaction to investigate the underlying mechanism of the photocatalysts of $ZnCo_2O_4$-$Zn(OH)_2$ microspheres during the photodegradation of MV or TC solution, as shown in Figure 13a and b. Isopropyl alcohol (IPA), L-ascorbic acid (AA), triethanolamine (TEOA), and silver nitrate ($AgNO_3$) were utilized as scavengers to impede hydroxyl radicals (·OH), superoxide radical anions ($\cdot O_2^-$), holes (h^+), and electrons (e^-), respectively [43–46]. Adding IPA and AA scavengers to the photocatalytic reaction leads to a notable reduction in the photocatalytic efficiency. This outcome provides evidence that hydroxyl radicals (·OH) and superoxide radicals ($\cdot O^{2-}$) are the primary active species involved in the photodegradation of TC. Potential reactions that may occur during the photocatalytic degradation of MV or TC solutions over $ZnCo_2O_4$-$Zn(OH)_2$ microspheres can be outlined as a schematic diagram, as shown in Figure 13c. When the $ZnCo_2O_4$-$Zn(OH)_2$ microspheres are exposed to UVC light with photon energy (hv) exceeding their band gap, an electron (e^-) in the valence band (VB) can be promoted to the conduction band (CB), creating a hole in the VB and generating electron-hole pairs. Photogenerated electrons can interact with oxygen molecules on the surface, forming superoxide radical anions ($\cdot O_2^-$). These can then react with water molecules absorbed on the surface, producing hydroxyl radicals (·OH). Moreover, the photogenerated holes may combine with H_2O molecules, causing their dissociation into ·OH radicals. These superoxide radical anions and hydroxyl radicals are recognized as potent oxidants responsible for the decomposition of MV or TC molecules.

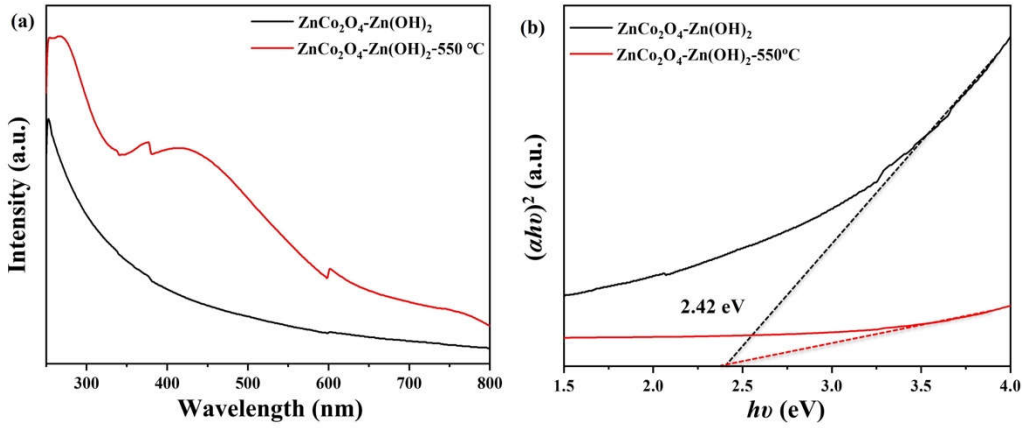

Figure 12. (a) UV-vis spectra and (b) Tauc plot of $ZnCo_2O_4$-$Zn(OH)_2$ microspheres and $ZnCo_2O_4$-$Zn(OH)_2$ microspheres (550 °C).

Preprints.org (www.preprints.org) | NOT PEER-REVIEWED | Posted: 29 July 2024 doi:10.20944/preprints202407.2266.v1

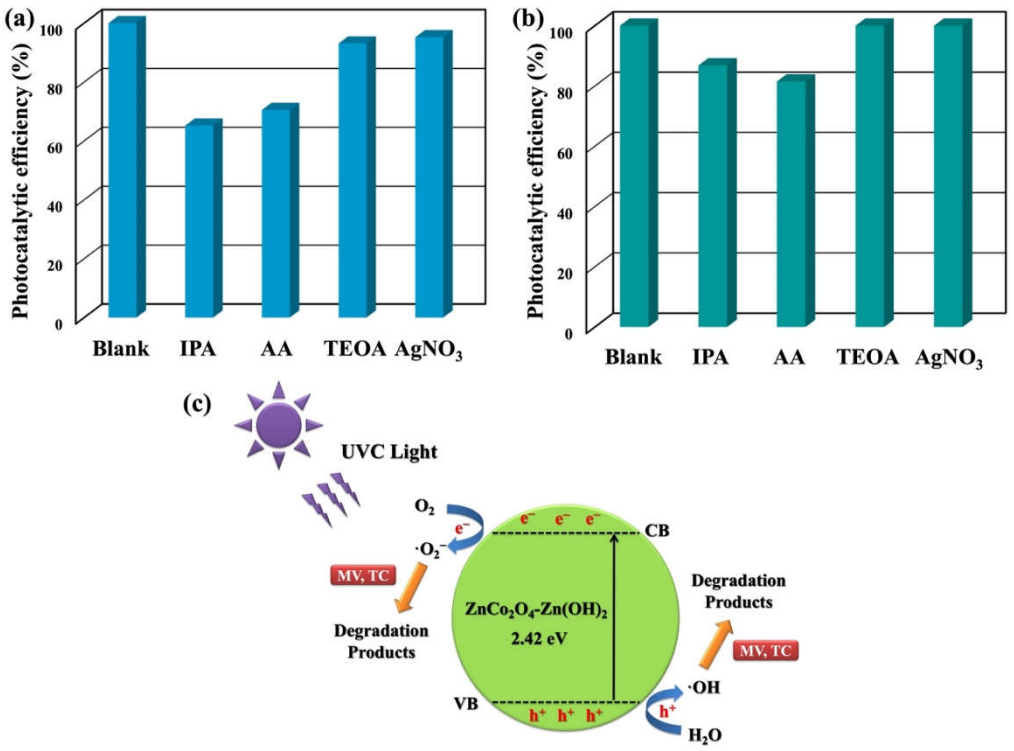

Figure 13. Photocatalytic activities of $ZnCo_2O_4$-$Zn(OH)_2$ microspheres (550 °C) for (a) MV and (b) TC solutions with four scavengers under UVC light irradiation. (c) Illustration depicting the electron transfer process of $ZnCo_2O_4$-$Zn(OH)_2$ microspheres under the UVC light irradiation.

3. Materials and Methods

3.1. Materials and Chemicals

Carbon cloth was procured from As One International (Santa Clara, CA, USA) as a commercial source. The chemicals were sourced from commercial suppliers and were used without requiring additional purification. Sulfuric acid (H_2SO_4, 95-97%), hydrogen peroxide (H_2O_2, 35%), isopropanol (C_3H_8O, 95%), and ethanol (C_2H_5OH, 99.5%) were acquired from Echo Chemical (Miaoli County, Taiwan). Zinc nitrate hydrate ($Zn(NO_3)_2{\cdot}6H_2O$, 98%), cobalt(II) nitrate hexahydrate ($Co(NO_3)_2{\cdot}6H_2O$, 98%), ammonium fluoride (NH_4F, 98%), methyl violet ($C_{24}H_{28}N_3Cl$, 99.5%), urea (CON_2H_4, 99%), triethanolamine (TEOA, $C_6H_{15}NO_3$, 99+%), and L-ascorbic acid ($C_6H_8O_6$, 99%) were acquired from Sigma-Aldrich (Darmstadt, Germany). Tetracycline (250 mg) was acquired from TWi Pharmaceuticals (Taipei City, Taiwan). Deionized (DI) water with a resistivity exceeding 18.3 MΩ was used to prepare all reaction solutions.

3.2. Fabrication of $ZnCo_2O_4$-$Zn(OH)_2$ Microspheres

The carbon cloth is cut into (1.5*2.5 cm) sizes, soaked in a volume ratio of hydrogen peroxide and sulfuric acid (3:7) for 15 min, then thoroughly rinsed with DI water, and dried in an oven at 75°C for 5 h. $ZnCo_2O_4$-$Zn(OH)_2$ microspheres were prepared using a facile hydrothermal approach on carbon cloth. A solution consisting of 0.75 mmol of $Zn(NO_3)_2{\cdot}6H_2O$, 1.5 mmol of $Co(NO_3)_2{\cdot}6H_2O$, 1.5 mM of NH_4F, and 3.75 mM of urea was prepared in 30 mL of DI water and stirred magnetically for 20 minutes. Subsequently, the carbon cloth, having undergone prior preparation, was immersed in this homogenous mixture and maintained at 120 °C for 5 h. Once the temperature returned to ambient, the $ZnCo_2O_4$-$Zn(OH)_2$ microspheres were washed with DI water and ethanol and desiccated at 75 °C for the entire night. The specimen was calcinated at varying temperatures for 2 h under atmospheric pressure.

 doi:10.20944/preprints202407.2266.v1

3.3. Characterization

Various analytical techniques thoroughly examined the microstructures and elemental composition of the as-synthesized $ZnCo_2O_4$-$Zn(OH)_2$ microspheres. Field-emission scanning electron microscopy (FESEM) was performed utilizing a Hitachi S-4800 instrument from Japan. Field emission transmission electron microscopy (FETEM) was employed utilizing a JEOL-2100F instrument manufactured in Japan, outfitted with energy-dispersive X-ray spectroscopy (EDS) to analyze the primary components. X-ray diffraction (XRD) analysis was conducted utilizing a Bruker D2 instrument in the United States to examine the crystal structures of the fabricated substrates. The elemental chemical compositions of the $ZnCo_2O_4$-$Zn(OH)_2$ microspheres were analyzed through X-ray photoelectron spectroscopy (XPS) utilizing a ULVAC-PHI PHI 5000 VersaProbe instrument manufactured in Japan..

3.4. Photocatalytic Measurement

The efficiency of photocatalytic materials was assessed through the disintegration of a methyl violet solution (0.01 mM) and tetracycline (0.1 mM) without altering the pH levels. During the standard photocatalytic activity, a UVC lamp emitting 253.7 nm with a power of 10 W from Philips in Amsterdam served as the illumination source. Changes in the distinctive absorption bands of the methyl violet and tetracycline solutions were monitored via a UV-vis spectrophotometer (Hitachi U-2900, Tokyo, Japan). When exposed to UVC lamp illumination, these photocatalysts' effectiveness was quantified by the ratio C/C_0, where C_0 represents the solutions' initial concentrations, and C denotes their concentrations at specific instances.

4. Conclusions

$ZnCo_2O_4$-$Zn(OH)_2$ microspheres were effectively created on a carbon cloth using a facile hydrothermal method. The surface features of these microspheres and their ability to break down methyl violet were enhanced by adjusting the thermal annealing temperatures. This temperature adjustment was key in modifying the porosity of the $ZnCo_2O_4$-$Zn(OH)_2$ microspheres, improving their photocatalytic abilities. The thermally annealed $ZnCo_2O_4$-$Zn(OH)_2$ microspheres showed increased specific surface area and light absorption compared to untreated ones, making them highly effective UVC-light-exposed photocatalysts. Further studies confirmed the microspheres' superior performance as reusable photocatalysts for degrading MV and TC. Trapping experiments identified superoxide and hydroxyl radicals as the major reactive species in the photodegradation process involving $ZnCo_2O_4$-$Zn(OH)_2$ microspheres. $ZnCo_2O_4$-$Zn(OH)_2$ microspheres offer a cost-effective and efficient photocatalytic solution with potential applications across various disciplines due to their simplicity, high efficiency, and reusability.

Author Contributions: Conceptualization, Y.-C.C.; methodology, S.-J.J., N.-C.C.; software, Y.-C.C.; validation, S.-J.J., N.-C.C., and C.-M.C.; formal analysis, S.-J.J., N.-C.C., and C.-M.C.; investigation, Y.-C.C.; resources, C.-M.C. and Y.-C.C.; data curation, S.-J.J., N.-C.C., and C.-M.C.; writing—original draft preparation, Y.-C.C.; writing—review and editing, Y.-C.C.; visualization, S.-J.J., N.-C.C., and C.-M.C.; supervision, Y.-C.C.; project administration, Y.-C.C.; funding acquisition, Y.-C.C. All authors have read and agreed to the published version of the manuscript.

Funding: This research was funded by the National Science and Technology Council, Taiwan (NSTC 112-2221-E-035-017-MY3) and Taichung Veterans General Hospital, Taiwan (TCVGH-FCU1138202 and TCVGH-1135401C).

Institutional Review Board Statement: Not applicable.

Informed Consent Statement: Not applicable.

Data Availability Statement: No new data were created or analyzed in this study. Data sharing is not applicable to this article.

Acknowledgments: The authors appreciate the Precision Instrument Support Center of Feng Chia University for providing the fabrication and measurement facilities.

Conflicts of Interest: The authors declare no conflict of interest.

References

1. Chandrasekaran, S.; Bowen, C.; Zhang, P.; Li, Z.; Yuan, Q.; Ren, X.; Deng, L. Spinel photocatalysts for environmental remediation, hydrogen generation, CO2 reduction and photoelectrochemical water splitting. *J. Mater. Chem. A* **2018**, *6*, 11078-11104, doi:10.1039/C8TA03669A.
2. Sriram, B.; Baby, J.N.; Wang, S.-F.; George, M.; Joseph, X.B.; Tsai, J.-T. Surface Engineering of Three-Dimensional-like Hybrid AB2O4 (AB = Zn, Co, and Mn) Wrapped on Sulfur-Doped Reduced Graphene Oxide: Investigation of the Role of an Electrocatalyst for Clioquinol Detection. *ACS Applied Electronic Materials* **2021**, *3*, 362-372, doi:10.1021/acsaelm.0c00906.
3. Amirzhanova, A.; Akmanşen, N.; Karakaya, I.; Dag, Ö. Mesoporous MnCo2O4, NiCo2O4, and ZnCo2O4 Thin-Film Electrodes as Electrocatalysts for the Oxygen Evolution Reaction in Alkaline Solutions. *ACS Applied Energy Materials* **2021**, *4*, 2769-2785, doi:10.1021/acsaem.1c00064.
4. Zhang, G.; Li, C.; Cheng, F.; Chen, J. ZnFe2O4 tubes: Synthesis and application to gas sensors with high sensitivity and low-energy consumption. *Sens. Actuators. B Chem.* **2007**, *120*, 403-410, doi:https://doi.org/10.1016/j.snb.2006.02.034.
5. Kefeni, K.K.; Mamba, B.B. Photocatalytic application of spinel ferrite nanoparticles and nanocomposites in wastewater treatment: Review. *Sustainable Materials and Technologies* **2020**, *23*, e00140, doi:https://doi.org/10.1016/j.susmat.2019.e00140.
6. Kanazawa, T.; Kato, K.; Yamaguchi, R.; Uchiyama, T.; Lu, D.; Nozawa, S.; Yamakata, A.; Uchimoto, Y.; Maeda, K. Cobalt Aluminate Spinel as a Cocatalyst for Photocatalytic Oxidation of Water: Significant Hole-Trapping Effect. *ACS Catal.* **2020**, *10*, 4960-4966, doi:10.1021/acscatal.0c00944.
7. Gambini, M.; Mazzoni, S.; Vellini, M. The Role of Cogeneration in the Electrification Pathways towards Decarbonization. *Energies* **2023**, *16*, doi:10.3390/en16155606.
8. Maity, D.; Karmakar, K.; Pal, D.; Saha, S.; Khan, G.G.; Mandal, K. One-Dimensional p-ZnCo2O4/n-ZnO Nanoheterojunction Photoanode Enabling Photoelectrochemical Water Splitting. *ACS Applied Energy Materials* **2021**, *4*, 11599-11608, doi:10.1021/acsaem.1c02351.
9. Qu, F.; Thomas, T.; Zhang, B.; Zhou, X.; Zhang, S.; Ruan, S.; Yang, M. Self-sacrificing templated formation of Co3O4/ZnCo2O4 composite hollow nanostructures for highly sensitive detecting acetone vapor. *Sens. Actuators. B Chem.* **2018**, *273*, 1202-1210, doi:https://doi.org/10.1016/j.snb.2018.07.005.
10. Morán-Lázaro, J.P.; López-Urías, F.; Muñoz-Sandoval, E.; Blanco-Alonso, O.; Sanchez-Tizapa, M.; Carreon-Alvarez, A.; Guillén-Bonilla, H.; Olvera-Amador, M.D.; Guillén-Bonilla, A.; Rodríguez-Betancourtt, V.M. Synthesis, Characterization, and Sensor Applications of Spinel ZnCo2O4 Nanoparticles. *Sensors* **2016**, *16*, doi:10.3390/s16122162.
11. Kim, T.W.; Woo, M.A.; Regis, M.; Choi, K.-S. Electrochemical Synthesis of Spinel Type ZnCo2O4 Electrodes for Use as Oxygen Evolution Reaction Catalysts. *J. Phys. Chem. Lett.* **2014**, *5*, 2370-2374, doi:10.1021/jz501077u.
12. Wang, Y.; Ke, J.; Zhang, Y.; Huang, Y. Microwave-assisted rapid synthesis of mesoporous nanostructured ZnCo2O4 anode materials for high-performance lithium-ion batteries. *J. Mater. Chem. A* **2015**, *3*, 24303-24308, doi:10.1039/C5TA06949A.
13. Shih, G.-H.; Liu, W.-R. A facile microwave-assisted approach to the synthesis of flower-like ZnCo2O4 anode materials for Li-ion batteries. *RSC Adv.* **2017**, *7*, 42476-42483, doi:10.1039/C7RA07660F.
14. Liu, M.M.; Ma, S.Y.; Cai, Y.H.; Ma, N.N.; Wang, L.; Sheng, H. ZnO/ZnCo2O4 composite prepared by one-step hydrothermal method for high-performance ethylene glycol sensor. *Ceram. Int.* **2022**, *48*, 22305-22312, doi:https://doi.org/10.1016/j.ceramint.2022.04.235.
15. Rajesh, J.A.; Min, B.-K.; Kim, J.-H.; Kang, S.-H.; Kim, H.; Ahn, K.-S. Facile hydrothermal synthesis and electrochemical supercapacitor performance of hierarchical coral-like ZnCo2O4 nanowires. *J. Electroanal. Chem.* **2017**, *785*, 48-57, doi:https://doi.org/10.1016/j.jelechem.2016.12.027.
16. Wang, J.; Wang, G.; Wang, Y.; Hao, J.; Wang, S. Preparation of ZnCo2O4 porous nano-flower-like materials by one-step cryogenic hydrothermal method and study on their capacitive and photocatalytic properties. *J. Mater. Sci. - Mater. Electron.* **2023**, *34*, 531, doi:10.1007/s10854-023-09896-5.
17. Zinatloo-Ajabshir, S.; Heidari-Asil, S.A.; Salavati-Niasari, M. Recyclable magnetic ZnCo2O4-based ceramic nanostructure materials fabricated by simple sonochemical route for effective sunlight-driven photocatalytic degradation of organic pollution. *Ceram. Int.* **2021**, *47*, 8959-8972, doi:https://doi.org/10.1016/j.ceramint.2020.12.018.
18. Peng, Q.; Liu, S.; Mao, Y.; Liu, X. Preparation of ZnCo2O4/BiVO4 Z-Scheme heterostructures to enhance photocatalytic performance in organic pollutant and antibiotic removal. *Colloids Surf. A Physicochem. Eng. Asp.* **2022**, *655*, 130165, doi:https://doi.org/10.1016/j.colsurfa.2022.130165.
19. Kitchamsetti, N.; Narsimulu, D.; Chinthakuntla, A.; Shilpa Chakra, C.; de Barros, A.L.F. Bimetallic MOF derived ZnCo2O4 nanocages as a novel class of high performance photocatalyst for the removal of organic pollutants. *Inorg. Chem. Commun.* **2022**, *144*, 109946, doi:https://doi.org/10.1016/j.inoche.2022.109946.

20. Pan, J.H.; Dou, H.; Xiong, Z.; Xu, C.; Ma, J.; Zhao, X.S. Porous photocatalysts for advanced water purifications. *J. Mater. Chem.* **2010**, *20*, 4512-4528, doi:10.1039/B925523K.
21. Wang, J.; Wang, G.; Wang, S.; Hao, J.; Liu, B. Preparation of ZnCo2O4 Nanosheets Coated on evenly arranged and fully separated Nanowires with high capacitive and photocatalytic properties by a One-Step Low-Temperature Water bath method. *ChemistrySelect* **2022**, *7*, e202200472, doi:https://doi.org/10.1002/slct.202200472.
22. Gnanamoorthy, G.; Karthikeyan, V.; Ali, D.; Kumar, G.; Jenifer, S.G.; Yadav, V.K.; Choudhary, N.; Narayanan, V. Realization of rGO/ZnCo2O4 nanocomposites enhanced for the antimicrobial, electrochemical and photocatalytic activities. *Diamond and Related Materials* **2021**, *120*, 108677, doi:https://doi.org/10.1016/j.diamond.2021.108677.
23. Liu, B.; Zhang, J.; Wang, X.; Chen, G.; Chen, D.; Zhou, C.; Shen, G. Hierarchical Three-Dimensional ZnCo2O4 Nanowire Arrays/Carbon Cloth Anodes for a Novel Class of High-Performance Flexible Lithium-Ion Batteries. *Nano Lett.* **2012**, *12*, 3005-3011, doi:10.1021/nl300794f.
24. Liu, T.; Wang, W.; Yi, M.; Chen, Q.; Xu, C.; Cai, D.; Zhan, H. Metal-organic framework derived porous ternary ZnCo2O4 nanoplate arrays grown on carbon cloth as binder-free electrodes for lithium-ion batteries. *Chem. Eng. J.* **2018**, *354*, 454-462, doi:https://doi.org/10.1016/j.cej.2018.08.037.
25. Chen, P.; Xu, K.; Fang, Z.; Tong, Y.; Wu, J.; Lu, X.; Peng, X.; Ding, H.; Wu, C.; Xie, Y. Metallic Co4N Porous Nanowire Arrays Activated by Surface Oxidation as Electrocatalysts for the Oxygen Evolution Reaction. *Angew. Chem. Int. Ed.* **2015**, *54*, 14710-14714, doi:https://doi.org/10.1002/anie.201506480.
26. Manjunatha, R.; Yuan, J.; Hongwei, L.; Deng, S.-Q.; Ezeigwe, E.R.; Zuo, Y.; Dong, L.; Li, A.; Yan, W.; Zhang, F.; et al. Facile carbon cloth activation strategy to boost oxygen reduction reaction performance for flexible zinc-air battery application. *Carbon Energy* **2022**, *4*, 762-775, doi:https://doi.org/10.1002/cey2.189.
27. Chen, R.; Wang, H.-Y.; Miao, J.; Yang, H.; Liu, B. A flexible high-performance oxygen evolution electrode with three-dimensional NiCo2O4 core-shell nanowires. *Nano Energy* **2015**, *11*, 333-340, doi:https://doi.org/10.1016/j.nanoen.2014.11.021.
28. Ma, T.Y.; Ran, J.; Dai, S.; Jaroniec, M.; Qiao, S.Z. Phosphorus-Doped Graphitic Carbon Nitrides Grown In Situ on Carbon-Fiber Paper: Flexible and Reversible Oxygen Electrodes. *Angew. Chem. Int. Ed.* **2015**, *54*, 4646-4650, doi:https://doi.org/10.1002/anie.201411125.
29. Okhay, O.; Tkach, A.; Gallo, M.J.H.; Otero-Irurueta, G.; Mikhalev, S.; Staiti, P.; Lufrano, F. Energy storage of supercapacitor electrodes on carbon cloth enhanced by graphene oxide aerogel reducing conditions. *Journal of Energy Storage* **2020**, *32*, 101839, doi:https://doi.org/10.1016/j.est.2020.101839.
30. Li, L.; Gao, J.; Cecen, V.; Fan, J.; Shi, P.; Xu, Q.; Min, Y. Hierarchical WS2@NiCo2O4 Core–shell Heterostructure Arrays Supported on Carbon Cloth as High-Performance Electrodes for Symmetric Flexible Supercapacitors. *ACS Omega* **2020**, *5*, 4657-4667, doi:10.1021/acsomega.9b04434.
31. Wang, H.-F.; Tang, C.; Wang, B.; Li, B.-Q.; Cui, X.; Zhang, Q. Defect-rich carbon fiber electrocatalysts with porous graphene skin for flexible solid-state zinc–air batteries. *Energy Storage Materials* **2018**, *15*, 124-130, doi:https://doi.org/10.1016/j.ensm.2018.03.022.
32. Kordek, K.; Jiang, L.; Fan, K.; Zhu, Z.; Xu, L.; Al-Mamun, M.; Dou, Y.; Chen, S.; Liu, P.; Yin, H.; et al. Two-Step Activated Carbon Cloth with Oxygen-Rich Functional Groups as a High-Performance Additive-Free Air Electrode for Flexible Zinc–Air Batteries. *Advanced Energy Materials* **2019**, *9*, 1802936, doi:https://doi.org/10.1002/aenm.201802936.
33. Liu, Z.; Zhao, Z.; Wang, Y.; Dou, S.; Yan, D.; Liu, D.; Xia, Z.; Wang, S. In Situ Exfoliated, Edge-Rich, Oxygen-Functionalized Graphene from Carbon Fibers for Oxygen Electrocatalysis. *Adv. Mater.* **2017**, *29*, 1606207, doi:https://doi.org/10.1002/adma.201606207.
34. Lin, L.; Li, Q.; Nie, S.; Peng, X.; Hu, N. 3D ZnCo2O4 nanowires@MnO2 nanosheets core-shell structures grown on carbon cloth for excellent supercapacitor electrodes. *Ceram. Int.* **2016**, *42*, 19343-19348, doi:https://doi.org/10.1016/j.ceramint.2016.09.105.
35. Mariappan, C.R.; Kumar, R.; Vijaya Prakash, G. Functional properties of ZnCo2O4 nano-particles obtained by thermal decomposition of a solution of binary metal nitrates. *RSC Adv.* **2015**, *5*, 26843-26849, doi:10.1039/C5RA01937K.
36. Jeong, G.H.; Jang, H.S.; Yoon, J.C.; Lee, Z.; Yang, J.; Jang, A.R.; Ryu, G.H. Morphologically Controlled Synthesis of Reduced-Dimensional ZnO/Zn(OH)2 Nanosheets. *ACS Omega* **2022**, *7*, 35834-35839, doi:10.1021/acsomega.2c04108.
37. Jheng, B.-R.; Chiu, P.-T.; Yang, S.-H.; Tong, Y.-L. Using ZnCo2O4 nanoparticles as the hole transport layer to improve long term stability of perovskite solar cells. *Sci. Rep.* **2022**, *12*, 2921, doi:10.1038/s41598-022-06764-w.
38. Chen, H.-Y.; Chen, P.-C. P-type spinel ZnCo2O4 thin films prepared using sol-gel process. *Appl. Surf. Sci.* **2020**, *505*, 144460, doi:https://doi.org/10.1016/j.apsusc.2019.144460.
39. Chopra, I.; Roberts, M. Tetracycline Antibiotics: Mode of Action, Applications, Molecular Biology, and Epidemiology of Bacterial Resistance. *Microbiology and Molecular Biology Reviews* **2001**, *65*, 232-260, doi:10.1128/mmbr.65.2.232-260.2001.

40. Xu, L.; Zhang, H.; Xiong, P.; Zhu, Q.; Liao, C.; Jiang, G. Occurrence, fate, and risk assessment of typical tetracycline antibiotics in the aquatic environment: A review. *Science of The Total Environment* **2021**, *753*, 141975, doi:https://doi.org/10.1016/j.scitotenv.2020.141975.
41. Navalón, S.; Dhakshinamoorthy, A.; Álvaro, M.; Ferrer, B.; García, H. Metal–Organic Frameworks as Photocatalysts for Solar-Driven Overall Water Splitting. *Chem. Rev.* **2023**, *123*, 445-490, doi:10.1021/acs.chemrev.2c00460.
42. Suram, S.K.; Newhouse, P.F.; Gregoire, J.M. High Throughput Light Absorber Discovery, Part 1: An Algorithm for Automated Tauc Analysis. *ACS Combinatorial Science* **2016**, *18*, 673-681, doi:10.1021/acscombsci.6b00053.
43. Wang, Z.; Zhang, J.; Lv, J.; Dai, K.; Liang, C. Plasmonic Ag2MoO4/AgBr/Ag composite: Excellent photocatalytic performance and possible photocatalytic mechanism. *Appl. Surf. Sci.* **2017**, *396*, 791-798, doi:https://doi.org/10.1016/j.apsusc.2016.11.031.
44. Wang, Z.; Wang, K.; Li, Y.; Jiang, L.; Zhang, G. Novel BiSbO4/BiOBr nanoarchitecture with enhanced visible-light driven photocatalytic performance: Oxygen-induced pathway of activation and mechanism unveiling. *Appl. Surf. Sci.* **2019**, *498*, 143850, doi:https://doi.org/10.1016/j.apsusc.2019.143850.
45. Xu, D.; Shi, W.; Song, C.; Chen, M.; Yang, S.; Fan, W.; Chen, B. In-situ synthesis and enhanced photocatalytic activity of visible-light-driven plasmonic Ag/AgCl/NaTaO3 nanocubes photocatalysts. *Appl. Catal., B* **2016**, *191*, 228-234, doi:https://doi.org/10.1016/j.apcatb.2016.03.036.
46. Chang, Y.-C.; Tasi, C.-L.; Ko, F.-H. Construction of ZnIn2S4/ZnO heterostructures with enhanced photocatalytic decomposition and hydrogen evolution under blue LED irradiation. *Int. J. Hydrogen Energy* **2021**, *46*, 10281-10292, doi:https://doi.org/10.1016/j.ijhydene.2020.12.119.